RSC Advances

PAPER

View Article Online
View Journal | View Issue

Cite this: *RSC Adv.*, 2017, **7**, 23502

Cyto-toxicity, biocompatibility and cellular response of carbon dots–plasmonic based nano-hybrids for bioimaging†

A. N. Emam, *[ab] Samah A. Loutfy,[c] Amany A. Mostafa,[ab] H. Awad[d] and Mona B. Mohamed[ef]

In this study, hybrid carbon dots–plasmonic nanostructures including carbon dots/polyethyleneimine/gold (C-dots/PEI/Au), and carbon dots/polyethyleneimine/silver (C-dots/PEI/Ag) have been prepared using a microwave irradiation method. The prepared hybrid nanostructures have been characterized *via* optical spectroscopy, high resolution transmission electron microscopy (HRTEM), and X-ray diffraction (XRD). A remarkable enhancement in the optical parameters, such as absorptivity and quantum yield (QY), has been observed for the hybrid nanostructure compared to pure carbon dots. This plasmonic enhancement was more pronounced in the presence of silver (C-dots/PEI/Ag nanohybrid) than that of gold (C-dots/PEI/Au nanohybrid). This is referred to the low intrinsic loss and the degree of the overlap between the absorption spectra of silver nanoparticles and carbon dots. Furthermore, the bio-compatibility assay and cellular response on epithelial kidney (Vero) normal cell has been investigated. The results showed that the optimal dose of treatment is about ~200 μg ml^{-1} using both C-dots/PEI/Au or C-dots/PEI/Ag, nano-hybrids could be used safely in diagnostic bioimaging applications.

Received 3rd February 2017
Accepted 13th April 2017

DOI: 10.1039/c7ra01423f

rsc.li/rsc-advances

1. Introduction

Biomedical imaging is a rapidly expanding research area not only because of its importance in early-stage detection, screening, and imaging-guided therapies of life threatening diseases,[1] but also because it provides a valuable tool to probe cellular constituents.[2] Nowadays, there are numerous organic dyes such as, charge transfer dyes (CT dyes) and green fluorescent proteins (GFP) used for *in vivo* sensing and as fluorescence tags.[3–6] However, these fluorescent dyes present some disadvantages, such as, photobleaching, blinking, and short fluorescence lifetimes, among others. These lead researchers to search for new alternatives.[4,7] Semiconductor quantum dots (SQDs) have attracted much attention for their serving as probes in cell imaging and other biomedical applications. Compared to conventionally used organic dyes, SQDs have unique photophysical properties such as tunable emission wavelengths, large molar extinction coefficient and quantum efficiencies. Moreover, they have high resistance to both of photobleaching and chemical degradation.[4,8–11] As widely acknowledged, however, the traditional SQDs have a heavy metal core that prevents its application for *in vivo* assays.[12–14] In addition, the fluorescence blinking in single SQDs, is harmful for dynamic tracking due to information loss.[15,16]

Alternatively, during the last decade studying the photophysics of carbon dots (C-dots) as a new class of nanoparticles became a target for many research groups[17–19] due to their biocompatibility,[20] low toxicity,[21] water solubility[22] and high quantum yield.[18,20,22] In addition to its advantages are easy to synthesize[18,23–26] and functionalization of specific targeting.[27–29] Therefore, C-dots have huge potential as a new generation of luminescent materials superior to conventionally used fluorescent organic dyes or inorganic semiconductor quantum dots (SQDs).[30,31] The existence of many hydroxyl and/or carboxyl moieties on their surface facilitates their surface functionalization with various organic, polymeric, inorganic, or biological species.[32,33] This could influence their fluorescence properties.[27,33] Furthermore, C-dots have non-blinking characteristics, which allow single-molecule tracking compared to SQDs.[20,22,34] Therefore, nowadays it isn't surprising the use of C-dots in a multiple assays for bioimaging and optical sensing.[13,21,35–40]

Plasmonic nanoparticles (*i.e.* Au and Ag NPs) have unusual chemical and physical properties that make them suitable for many potential and promising applications such as optical

[a]*Refractories, Ceramics and Building Materials Department, National Research Centre, Cairo, Egypt. E-mail: ahmed.gsc.ndp@gmail.com*

[b]*Nanomedicine and Tissue Engineering Laboratory, Medical Research Centre of Excellence, National Research Centre (NRC), Cairo, Egypt*

[c]*Virology and Immunology Unit, Cancer Biology Department, National Cancer Institute, Cairo University, Cairo, Egypt*

[d]*Tanning Materials and Leather Technology Department, National Research Centre, Cairo, Egypt*

[e]*National Institute of Laser Enhanced Sciences (NILES), Cairo University, Cairo, Egypt*

[f]*Egyptian Nanotechnology Center (EGNC), Cairo University, Zayed City, Giza, Egypt*

† Electronic supplementary information (ESI) available. See DOI: 10.1039/c7ra01423f

sensing, imaging and biotechnology.[41–43] By controlling their particle size and shape let them have the capability of tuning their optical and electronic properties.[44] The optical properties of metallic nanoparticles are originated by the collective oscillation of conduction electrons that resulted from their interaction with electromagnetic radiation (*i.e.* light). This phenomenon is known as the localized surface plasmon resonance (LSPR).[45–47] That increases light harvesting and enhance the collective optical properties in metallic hybrid nanostructures.[48–50]

The addition of metallic nanoparticles *e.g.* Au and Ag NPs in direct contact with the C-dots or graphene quantum dots (GQDs) enhances the charge separation and the carrier mobility in these hybrid nanocomposites. Up to the authors' knowledge the coupling mechanism between the optical properties of the metallic nanoparticles with the C-dots and their influences on their absorption cross section and photoluminescence properties have not been studied yet. A few studies have been devoted to track the influence of plasmonic nanostructures on the photoluminescence (PLE) of C-dots.[51–56]

As reported in previous studies, polyethylenimine (PEI) has been used as an example of polymeric coating agent that able to aid in generating the C-dots with the strong photoluminescence properties. This is attributed to the successful introduction of nitrogen-containing organic molecules onto the surface of C-dots.[27,33,57,58]

In this study, water soluble nitrogen doped carbon dots (N-doped C-dots), and their nano-hybrids plasmonic nanoparticles such as, Au or Ag NPs in presence of PEI *e.g.* C-dots/PEI/Au or C-dots/PEI/Ag have been prepared for the sake of bioimaging application. The effect of the plasmonic nanostructures on the optical properties such as, optical absorptivity and the photoluminescence properties including quantum yield (QY) and full width at half maximum (FWHM) have been characterized either in presence or absence of PEI as dielectric polymeric spacer. Furthermore, the biocompatibility test and the cellular response on Vero normal cell have been tested. Finally, the live cell imaging has been scanned on human liver cancerous cells (HepG-2).

2. Results and discussion

2.1. Physicochemical properties of highly fluorescent carbon dots

Nitrogen doped water soluble carbon dots (N-doped C-dots) were prepared *via* facile synthetic method based on microwave irradiation method as mentioned previously. The obtained crude is attributed to complete polymerization of citric acid as a sole carbon source. Meanwhile, the existence of nitrogen dopant leads to increase the glistening of their aqueous solution.[59]

Fig. 1 presents the absorption and emission spectra of the as-prepared C-dots. The absorption spectrum (Fig. 1, solid-line) shows two significant bands, which located at 240 nm corresponding to 5.17 eV and 347.8 nm corresponding to 3.57 eV, respectively. Generally, the UV-Vis optical absorption in C-dots is originated from two kinds of optical transitions, as reported previously.[18,20,60–67] In our experimental results, the absorption

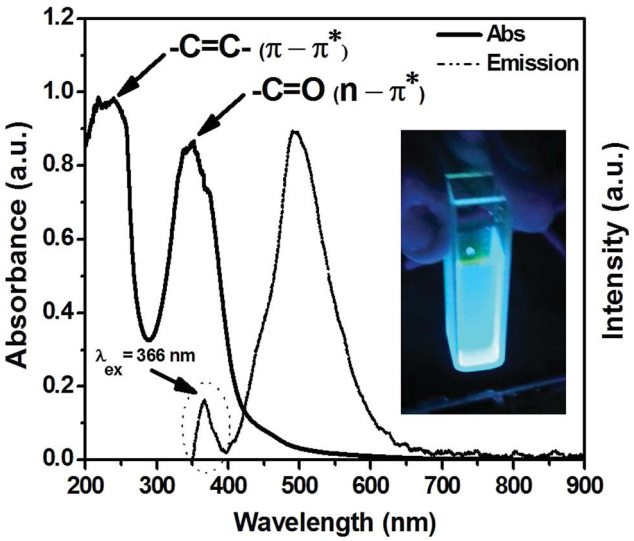

Fig. 1 The optical properties include both of absorption (solid-line) and emission spectra (dashed-line) under the steady-state conditions. The inset is the photograph for an aqueous solution of C-dots illuminated by a UV-lamp with λ_{ex} = 366 nm light.

spectra showed two characteristics spectral features, the first one was at 240 nm that could be assigned to π–π* transition of aromatic –C=C–, and –C–C– bonds in the sp^2 hybridized domain of graphitic core. The second one was at 347.8 nm that attributed to n–π* transition of –C=O, C–N or –C–OH bonds in the sp^3 hybridized domains, which originated from carboxyl (–COOH) or amine ($-NH_2$) groups exists on C-dots surface. It's reported that the π–π* transitions couldn't produce any noticeable fluorescence signal. However, the n–π* should have more prominent impact on the photophysical properties especially the PLE signals.[60–65] In addition, Qu *et al.* assumed that the high energy tail is extended into the visible region of the absorption spectrum due to Mie scattering caused by nanoparticles.[68]

A strong and ultra-bright fluorescence signal at 488 nm is observed upon their optical excitation using UV-lamp irradiation at 366 nm, as shown in Fig. 1 (dashed circle). Finally, the large stokes shift between both absorption and emission spectra about ~140.02 nm was observed. Xiaohui *et al.* suggested that this large stokes shift may be attributed to the strong interaction between the excited dipole moments in C-dots, and the nearby water molecules (*i.e.* polar solvent).[69] It's beleived that, this large Stokes shift might be due to the nature of the emitting state in carbon dots, which is the triplet state not the excited singlet state.[70]

The morphological and structural properties of the as-prepared C-dots were confirmed by using HR-TEM and XRD as shown in Fig. 2(a and b). TEM micrograph shows that C-dots are spherical and relatively narrow size distribution. The average particle size of the as-prepared C-dots is distributed in the range from 6.5 ± 2 nm (Fig. 2(a)). However, the HR-TEM and the corresponding fast Fourier transform (FFT) micrograph show that most particles are observed to be quasi-crystalline carbon particles with a slight appearance of lattices (inset in Fig. 2(a)); which was in a good agreement of other previously reported

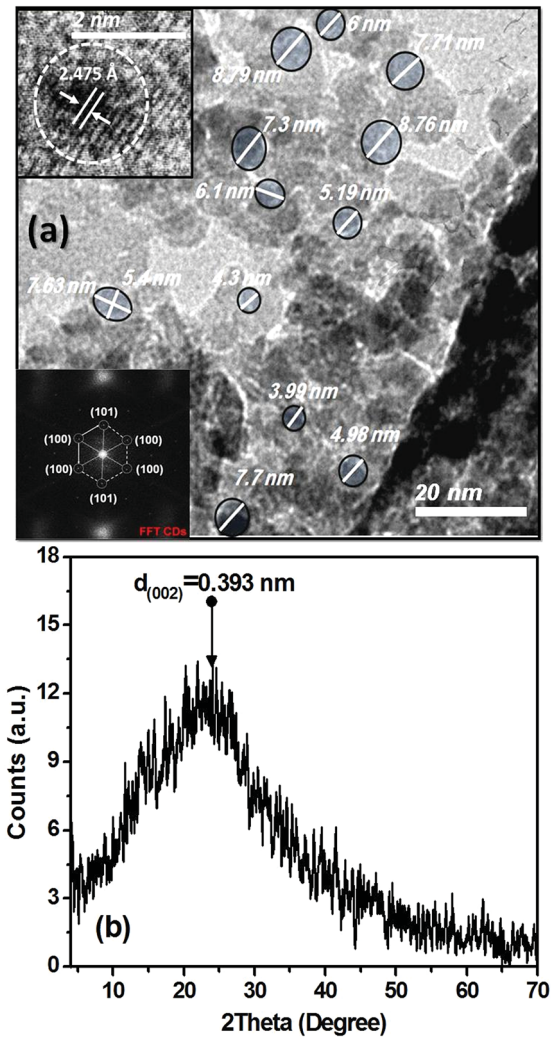

Fig. 2 (a) TEM micrograph and (b) XRD patterns of the as-prepared C-dots. The insets into (a) are the HR-TEM (upper left), and the corresponding FFT patterns (lower-left) of C-dots calculated *via* ImageJ software.

observations.[38–40,71] In these studies, rare particles possess well-resolved lattice fringes (the insets in Fig. 2(a)).[38–40,71] The well-resolved lattice fringes with an inter-planar spacing about 2.475 Å were observed in (Fig. 2(a), upper left inset), which is close to the (100) facet of sp^2-graphitic carbon,[38–40,71,72] and (1120) facet of hexagonal patterns of graphene.[73]

XRD patterns as depicted in Fig. 2(b) display a weak broad reflection at position of around 2θ 22.59°, suggesting the lattice-spacing distance (d_{hkl}) of 3.93 Å, which reveals to (002) crystallographic reflection of the hexagonal bulk-graphite.[23,25,60,73,74] The reason for the low intensity and broadness for XRD patterns of the as-prepared C-dots, in addition their shift to lower 2θ angle about ~22.59° compared to bulk-graphite around 26.543° are attributable to the small crystallite size as well as resulting stress and strain effects. Moreover, the bonding between the carbon layers is limited to weak van der Waals interactions; the shift of XRD patterns is most obvious for (*hkl*) indices of the (001) type.[74] Liang and co-workers reported that the weakness in the reflection intensity, and larger in inter-planer spacing than that of graphite (3.36 Å) is attributed to the existence of more functional groups. This indicates increasing in the amorphous nature attributed to the introduction of more oxygen containing groups.[23,60,73,74]

2.2. Influence of plasmonic coupling on the PLE properties of carbon dots (C-dots)

Plasmonic/polymeric spacer/C-dots hybrid nanocomposites were prepared *via* physical conjugation of surface coated C-dots to polymeric materials (*i.e.* PEI 1200) to plasmonic nanostructures (*i.e.* Au or Ag NPs), as shown in Scheme 1. In this preparative scheme, we followed two steps to fabricate these hybrid nanocomposites. The first step is the successful coating of C-dots with dielectric polymeric spacer such as; PEI, based on Han *et al.* method.[75] Whereas, the second step was related to the incubation of plasmonic NPs with PEI coated C-dots for physical conjugation in a volumetric ratio (*i.e.* plasmonic NPs : C-dots) within a range from 1 : 1 to 1 : 20. Such nanocomposites

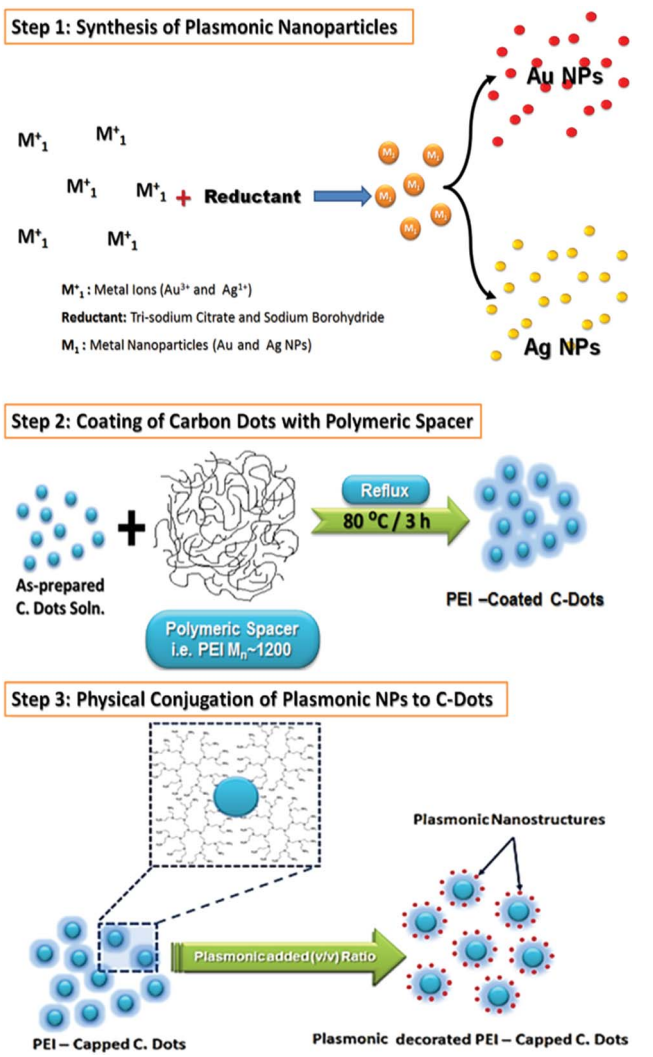

Scheme 1 Fabrication of plasmonic–carbon dots hybrid nanocomposites.

showed a stable and clear solution even after three months after the preparation (see Fig. S1, ESI†). This is attributed to electrostatic interactions between the plasmonic nanostructures with hydroxyl, amine, and other functional groups functionalized C-dots. Since this type of interactions could be act as the driving force for the assembly of C-dots/PEI onto plasmonic nanoparticles. In addition, C-dots/PEI might be playing the role of a stabilizing agent, which prevent both of Ag NPs or Au NPs from the aggregation. Moreover, an assembly of well-separated C-dots on the plasmonic nanostructures can be provided at low content of the plasmonic nanostructures with a strongly attached to their surface even after centrifugation.

HR-TEM images and XRD patterns had been recorded for the hybrid plasmonic–carbon dots nanocomposites as shown in Fig. 3 and 4. It is very obvious in Fig. 3(a and c) that the metallic part is in close proximity to the carbon dot. While in the presence of PEI, a space between the metallic part and the carbon dot is clear as shown in Fig. 3(b and d). The average thickness of the spacer is found to be 4–6 nm, Fig. 3(b and d). Furthermore, the crystallographic structure of these hybrid nanostructures was compared to pure C-dots, as shown in Fig. 4. XRD patterns for C-dots/Au hybrid nanostructures exhibits three reflection patterns within the range from 38 to 64.6°, due to the (111), (200) and (200) crystallographic plans of gold nanoparticles at 38.01°, 45.07° and 64.63°, respectively. Whereas in case of C-dots/Ag hybrid nanostructures accompanied with a broad band at 22.8° due to the (002) crystallographic reflection of sp^3 of graphite core, three sharp and significant diffraction patterns were observed. These reflections were recorded at 38.13, 44.05 and 64.67° corresponding to (111), (200) and (220) reflection plans of silver nanoparticles.

Furthermore, the hydrodynamic diameter (H_D) in a vehicle solution, for C-dots, C-dots/PEI, C-dots/PEI/Au and C-dots/PEI/Ag was determined using dynamic light scattering (DLS) technique, (Fig. S2, ESI†). C-Dots showed the smallest size, where the hydrodynamic diameter (H_D) was about 56.54 nm with a polydispersity index (PDI) 0.503, as shown in (Fig. S2a†). However, in the case of C-dots/PEI, the H_D increased and extended to 85.14 nm with a polydispersity index (PDI) 0.774, as shown in (Fig. S2b†). When C-dots/PEI conjugated with plasmonic nanostructures such as, Au and Ag NPs, hybrid nanocomposites of C-dots/PEI/Au and C-dots/PEI/Ag were formed. The average diameter was extended to 91.88 with PDI ~0.879 and 132.1 nm with PDI ~0.664, respectively (see Fig. S2c and S2d†).

Fig. 5 shows the influence of the plasmonic on the absorption spectra of carbon dots. Fig. 5(a) shows the absorption spectra of pure carbon, pure carbon dots capped with the PEI as spacer, pure silver nanoparticles and pure gold nanoparticles. The presence of plasmonic nanoparticles close to C-dots has remarkable influence on the absorption spectra of the carbon dots either in presence of PEI as spacer or not.

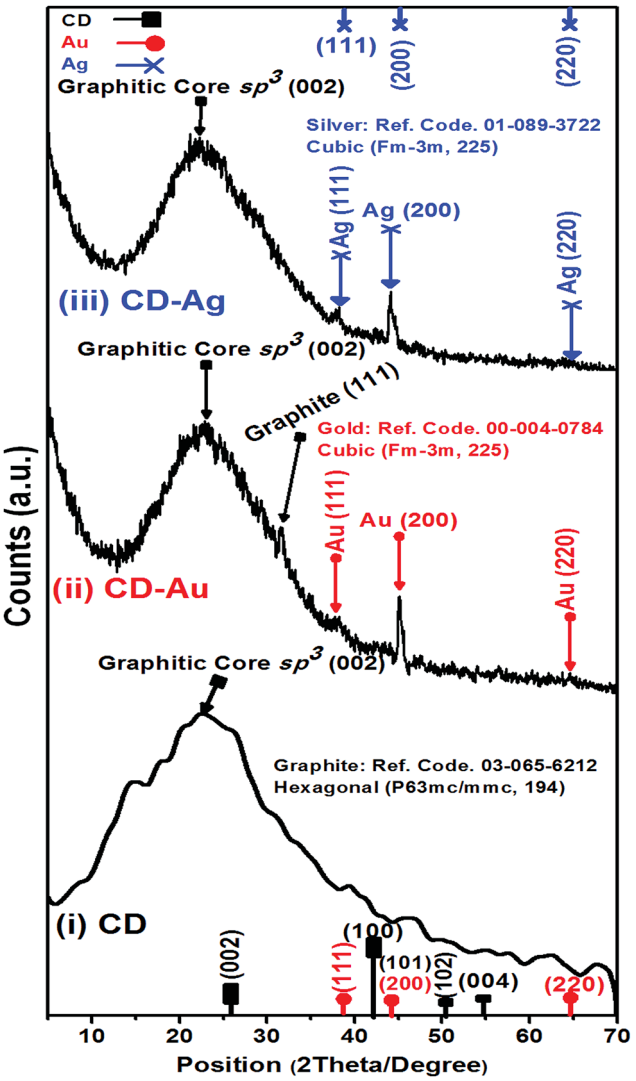

Fig. 4 XRD patterns for (i) pure C-dots (ii) C-dots@Au, and (iii) C-dots@Ag hybrid nanocomposites.

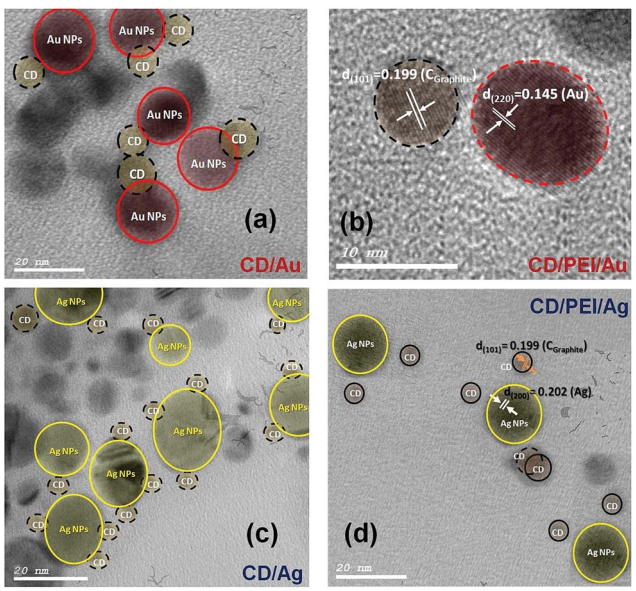

Fig. 3 TEM micrographs of (a) C-dots@Au, (b) C-dots@PEI@Au, (c) C-dots@Ag and (d) C-dots@PEI@Ag hybrid nanocomposites.

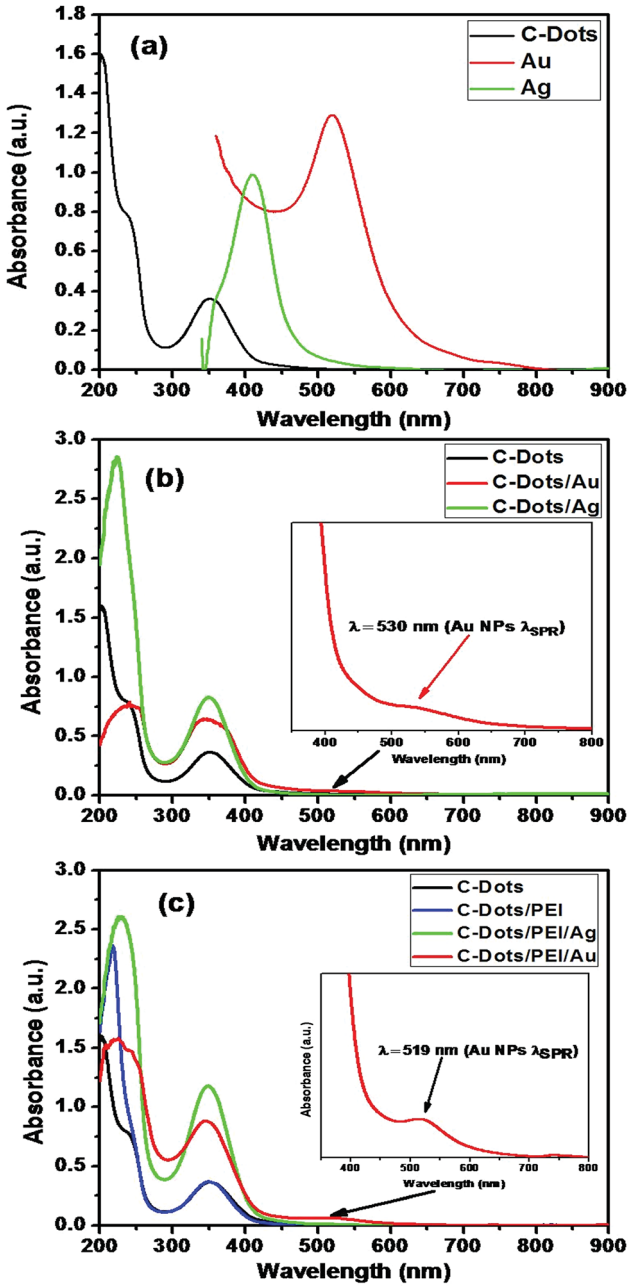

Fig. 5 Absorption spectra for each of (a) naked C-dots, Ag and Au NPs, respectively. (b) C-Dots, C-dots@Ag and C-dots@Au nanohybrid, and (c) naked C-dots, C-dots@PEI, C-dots@PEI@Ag and C-dots@PEI@Au nanohybrids.

Fig. 5(b and c) show the effect of the gold or silver nanoparticles on the absorption spectra of carbon dots in absence and in-presence of PEI as spacer. It is clear that presence of plasmonic increase the absorption coefficient and absorption cross-section of the C-dots. This is due to the enhancement of the interaction with light near the metal surface due to the enhancement of local fields associated with the surface plasmon (SP) of the metallic part. This effect could enhance the fluorescence of the C-dot part significantly.[76,77] The second process is the dumping of the surface plasmon absorption band of the metallic part, which could be due to either energy transfer between the C-dots and the metallic parts or electron transfer from the C-dots to the metal.[78]

The PLE properties of plasmonic@C-dots have been investigated in presence of dielectric polymeric spacer such as, PEI as shown in Fig. 6. The PLE parameters such as quantum yield, FWHM and the enhancement factor are listed in Table 1 in case of C-dot/spacer/Ag and C-dot/spacer/Au hybrid nanostructures, respectively. It is clear that, a tremendous enhancement in the PLE intensity of C-dots upon their conjugation with plasmonic nanostructures in the presence of PEI as dielectric polymeric

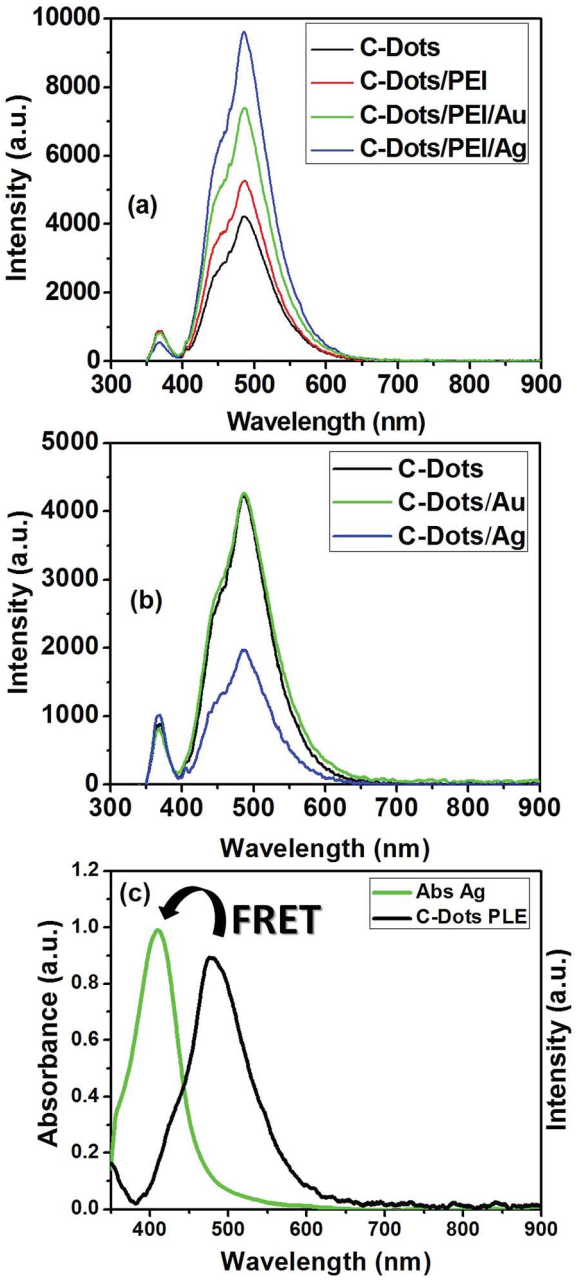

Fig. 6 Effect of plasmonic NPs on the PLE features of C-dots; (a) in presence or (b) in absence of spacer (*i.e.* PEI) upon excitation at steady-state condition (*i.e.* 366 nm). (c) Spectral overlapping between PLE spectra C-dots (black line) and the adsorption spectrum of Ag NPs (green line).

Table 1 Influence of plasmonic nanoparticles (Au and Ag NPs) on the PLE properties of C-dots in presence or absence of polymeric spacer (*i.e.* PEI)

Sample	At λ_{ex}[a] 366 nm		QY/QY_{dye}[d] (steady-state)	FWHM[e] (steady-state)
	I[b]	I/I_0[c]		
CD	(I_0) **4223.69**	—	**22.468**	**33.60484**
CD/Au	4683.54	1.11	36.40	86.74477
CD/PEI/Au	**7403.64**	**1.75**	**55.52**	**30.56937**
CD/Ag	1833.45	0.434	8.723	2.5756916
CD/PEI/Ag	**9134.23**	**2.16**	**77.213**	**17.44447**

[a] λ_{ex}: excitation wavelength. [b] λ_{em}: PLE wavelength. [c] I/I_0: relative enhancement factor. [d] QY/QY_{dye}: relative quantum yield. [e] FWHM: full width at half-maximum.

spacers under steady-state excitation, as shown in Fig. 6(a). Moreover, it is noticeable that the enhancement factor (I/I_0) and the quantum yield in case of C-dot/spacer/silver hybrid nanostructure is much more than that of the corresponding gold hybrid nanostructure as shown in Fig. 6(a). In contrast, C-dot/silver nano-hybrid showed a dramatic quenching in the fluorescence of carbon dots than in case of C-dot/Au nano-hybrid, which shows a little enhancement in the fluorescence intensity of the C-dots, as illustrated in Fig. 6(b). This quenching is owing to Forster resonance energy transfer (FRET) originated from spectral overlap between the emission spectrum of the C-dots which act as a donor, and the absorption spectrum of silver nanoparticles that act as an acceptor. As shown in Fig. 6(c), the fluorescence emission spectrum of C-dots has a good overlap with the absorption spectrum of Ag NPs, suggesting that an efficient energy transfer between them can take place.[52]

This could be explained as follow; silver is advantageous for plasmonics because of low intrinsic losses that result in narrow surface plasmon resonances with high oscillator strengths and large optical field enhancements.[79,80] Gold is a very inert metal but has higher intrinsic losses than silver, especially in the short wavelength range of the visible spectrum, where inter-band transitions occur. Intrinsic losses dampen the surface plasmon and cause a broadening of surface plasmon resonances and lower quality factors.[81,82] A pronounced shoulder within the blue side of the steady-state PLE asymmetric spectral band appeared, upon the conjugation of metallic nanoparticles to polymeric coated C-dots. The enhancement in this shoulder is due to metal enhancement fluorescence (MEF) effect. This effect is a result from the combined effects of the creation of an electric field that induced an intense excitation field around the plasmonic in the vicinity of the C-dots. An increase in the intrinsic emission rate of the C-dots, and a strong coupling between the exciton in C-dots and the plasmons in the metal is observed.[83] This strong exciton-plasmonic coupling is due to the fact that the surface plasmon resonance of Ag NPs is very close to the absorption band of the C-dots, thus its influence is more than that of the gold nanoparticles which has absorption band in the red side of the C-dots absorption (off-resonance).

Additionally, C-dots, C-dots/PEI, C-dots/PEI/Au and C-dots/PEI/Ag had excellent stability, which their PLE intensity did not change even after storage of 3 months and UV-excitation for 3 h (see Fig. S3†).

It is obvious that capping C-dots with PEI does not alter the main absorption peak of C-dots at 348 nm, but affects slightly the high energy bands at the UV range (shoulder at ~236 nm & band at 217 nm) due to the strong absorption of the polymeric material in this region (Fig. 5(c)). This is indicating that PEI could be act as a secondary excitation source for C-dots, and facilitates the energy transfer through a plasmon-exciton coupling process.

To elucidate the rationale behind choosing of PEI over other polymeric coating agents, six different polymeric spacers have been used to the PLE properties of C-dots/plasmonic nanohybrids, as shown in (Fig. S4†). The PLE parameters such as quantum yield, FWHM and the enhancement factor are listed in Table S1† in case of C-dot/spacer/Au and C-dot/spacer/Ag hybrid nanostructures, respectively. It is clear that, a tremendous enhancement in the PLE intensity of C-dots upon the conjugation with plasmonic nanostructures such as, Au and Ag NPs in the presence of PEI than other used polymeric spacers under the steady-state excitation, as summarized in Fig. S4a and S4b and Table S1.† Where the fluorescence enhancement factor was about 1.75 and 2.16-fold that of C-dots for C-dots/PEI/Au and C-dots/PEI/Ag nanohybrids, respectively. Also, the FLQY was about 2.21-fold for C-dots/PEI/Au and 3.44-fold for C-dots/PEI/Ag that of C-dots.

The physical interpretation for both of fluorescence quenching and enhancement has been illustrated in Fig. 7. If the C-dots based-on fluorophores is located in a close proximity to the metallic surface, a non-radiative dumping due to either energy transfer between the C-dots and the metal or the electron transfer from C-dots to the metal (Fig. 7(a)).[84] Whereas the C-dots/plasmonic hybrid nanostructures are separated with dielectric spacer such as, polymer (*i.e.* distance increase), light–mater interactions will be enhanced near metal surface which based on the enhancement of local fields associated with the surface plasmon (SP) of the metallic part. This effect could

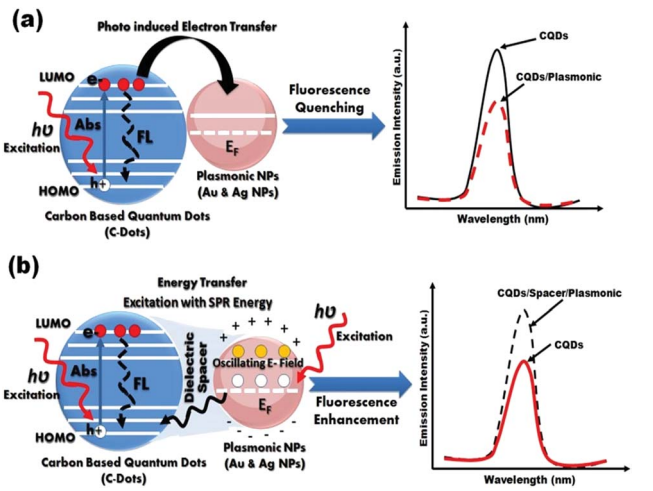

Fig. 7 Schematic illustration for possible mechanisms for fluorescence (a) quenching, and (b) enhancement in C-dots/plasmonic nano-hybrids.

enhance the fluorescence of the C-dots based-on fluorophores part significantly as shown Fig. 7(b).[55,76,77]

It is previously reported in the literature that the presence of intra-layer spacer between fluorescent C-dots and plasmonic NPs (*e.g.* Au or Ag NPs) is mainly responsible for whether it is PLE enhancement or quenching exists within the C-dots/plasmonic nanohybrids.[85–88] In the present study our results indicated that the conjugation to plasmonic gold nanoparticles shows an enhancement in PLE properties either in presence or absence of intra-layer spacing (*e.g.* PEI), which is total opposite to results reported by Dulkeith *et al.*[84] In contrast, Ag NPs only demonstrated an enhancement in the PLE properties for C-dots/PEI/Ag nanohybrids, compared to C-dots/Ag nanohybrids, which is contrast to Ran *et al.*[55] Finally, the obtained FL-QY of C-dots/PEI/Au and C-dots/PEI/Ag hybrid nanocomposites under the UV excitation at 366 nm are determined to be 55.52 and 77.213%, respectively. These values are considerably the highest FL-QY reported up till now.

2.3. Biocompatibility assay

Before the C-dots and its plasmonic hybrid nanocomposites were used for bio-imaging application, cellular biocompatibility experiments were evaluated using the MTT method. The purpose of performing biocompatibility test is to determine the fitness of these nanocomposites for biomedical imaging use, and to see whether use of the nanocomposites as a bioimaging contrast agents can have any potentially harmful cytotoxic effects.

Thus, biocompatibility assay was performed by the treatment of normal cell lines Vero cells as an *in vitro* test model of normal cell line to confirm this concept. In such study various concentrations of C-dots and their hybrid nanocomposites (200, 400, 600 and 800 μg ml^{-1}) are subjected to MTT screening colorimetric assay at 48 h time interval. In addition, plasmonic nanostructures (Au NPs & Ag NPs) were also screened for their cytotoxic effect at different concentrations (6.3, 12.5, 25, 50 and 100 μg ml^{-1}), (see Fig. S5†). Our results showed that C-dots/PEI nano-hybrids at concentration of 600 μg ml^{-1} could kill about 39% of cells, whereas when applied at concentration of 200 and 800 μg ml^{-1} killed only 8% of cells after 48 h of cell exposure (Fig. S5a†). Treatment of cells with 100 μg ml^{-1} Au NPs did not reveal any toxic effect, whereas treatment of cells with Ag NPs dramatically affected cells at the same concentration and became safe at concentration of 6 μg ml^{-1} after 48 h of cell exposure (Fig. S5b†).

Then, various concentrations of C-dots/PEI nano-hybrids conjugated with plasmonic nanostructures were also assessed in the same cell line. Results showed that C-dots/PEI nanohybrids when conjugated with Ag NPs (C-dots/PEI/Ag nanohybrids) was more toxic on cells than its conjugation with Au NPs (C-dots/PEI/Au nano-hybrids). Data are presented in Fig. S5c.† Treatment of cells with 200 μg ml^{-1} of C-dots/PEI/Au nano-hybrids could kill 10.5% of cells *versus* killing of 34% of cells when treated with C-dots/PEI/Ag nano-hybrids. Further insight analysis was performed to evaluate how much concentration of Ag NPs was associated with toxic effect of C-dots/PEI/Ag nano-hybrids. Results showed that when cells treated with 6.9 μg ml^{-1} of Ag NPs that used in the fabrication of 200 μg ml^{-1} C-dots/PEI/Ag nano-hybrids, could kill 34% of the cells. In contrast, cells treated with Au NPs at double concentration that used for Ag NPs (12.3 μg ml^{-1}) in the fabrication of 200 μg ml^{-1} C-dots/PEI/Au nano-hybrids, it killed only 10% of cells. This indicates that the cytotoxic effect of C-dots/PEI/Ag nano-hybrids is due to toxic effect of Ag NPs, as demonstrated in Table 2. The cytotoxic effect of cells treated with Ag NPs could be due to disturbances in cyto-skeletal functions as a result of release of Ag^{1+} ions, which involves disruption of the mitochondrial respiratory chain by Ag NPs leading to production of ROS and interruption of ATP synthesis, and ultimately DNA damage.[89,90] Thus, we can concluded that the exposure to lowest dose about 200 μg ml^{-1} possess good biocompatibility and low toxicity that are needed for bio-imaging.

Extensive evaluation to our fabricated nano-hybrids was performed to investigate response additivity approach using response additivity model (linear interaction effect),[91] which shows that a positive drug combination effect occurs when the observed combination effect (E_{AB}) is greater than the expected additive effect given by the sum of the individual effects (E_A + E_B). The Combination Index (CI) was calculated as in following equation:[91]

$$CI = \frac{E_A + E_B}{E_{AB}} \quad (1)$$

where, E_A and E_B are referring to the effect of each composite-individual, and the E_{AB} indicates to the effect of their combination. The resulting combination index (CI) theorem offers quantitative definition for additive effect (CI = 1), synergism (CI < 1), and antagonism (CI > 1) in drug combinations.[91,92] Such analysis was performed to confirm toxic effect of Ag NPs when combined with C-dots PEI nano-hybrids. Our analysis showed that at concentration of 600 μg ml^{-1} where concentration of Ag NPs used in nanohybrids fabrication was 20.6 μg ml^{-1}, CI was >1 and hence can be interpreted as antagonism confirming toxic effect of Ag NPs. Such CI showed to be decreased to <1 indicating synergetic effect at lower concentration (200 μg ml^{-1}) of C-dots/PEI nano-hybrids, where effect of Ag NPs was very low (6.8 μg ml^{-1}) (Table 3). This indicates that applying of C-dots/PEI nanohybrids conjugated with plasmonic nanostructures will be safe if applied at concentration of 200 μg ml^{-1} (see Fig. S5†). We concluded from these results that at the highest concentration of C-dots/PEI nano-hybrids (800 μg ml^{-1}) when conjugated with Au NPs, it showed a synergetic effect (*i.e.* CI < 1 (CI = 0.15)) (Table 3, Fig. S6†). This indicates that it can be used safely in diagnostic applications. In contrast to this figure, treatment of cells with the lowest dose of C-dots/PEI nano-hybrids conjugated with Ag NPs (~200 μg ml^{-1}) revealed a synergetic effect too (*i.e.* CI < 1 (CI = 0.61)), and then be used also in the diagnosis purposes.

2.3.1. Live cell imaging. To validate the fluorescence property and imaging application, C-dots, C-dots/PEI/Au and C-dots/PEI/Ag nanohybrids were used as the probes for fluorescence microscopy imaging with HepG2 human liver carcinoma as a targeted model cancer cell lines. In such study both of bright and fluorescence for live cells stained with nitrogen

Table 2 Effect of the content of plasmonic NPs in CD-plasmonic nanohybrids on the cell viability

Sample	Control	800 μg ml^{-1}	600 μg ml^{-1}	400 μg ml^{-1}	200 μg ml^{-1}
Case 1. Au NPs contents in CD/PEI/Au nanohybrids					
Au content	0	49.36	37.02	24.68	**12.34**
Viability (%)	100	74.4554	69.6287	69.5545	**89.5297**
Case 2. Ag NPs contents in CD/PEI/Ag nanohybrids					
Ag content	0	27.592	20.694	13.796	**6.898**
Viability (%)	100	46.5846	50.417	52.363	**66.7197**

Table 3 Combination index of carbon dots and their hybrid nanocomposites

Concentration (μg ml^{-1})	Sample	Effect% (A)	Effect% (B)	Sum effect% ($E_A + E_B$)	Combination effect% (E_{AB})	Combination index (CI)
800	CD/PEI	−41.9668 (CD)	37.399 (PEI)	−4.5678	7.8222 (CD/PEI)	−0.58395
	CD/PEI/Au	7.8222 (CDPEI)	−3.82224 (Au)	3.99996	25.5446 (CD/PEI/Au)	0.156587
	CD/PEI/Ag		69.350 (Ag)	77.1722	53.4154 (CD/PEI/Ag)	1.444756
600	CD/PEI	−74.1469 (CD)	38.052 (PEI)	−36.09	38.8181 (CD/PEI)	−0.92972
	CD/PEI/Au	38.8181 (CDPEI)	9.64775 (Au)	48.4659	30.3713 (CD/PEI/Au)	1.59578
	CD/PEI/Ag		69.350 (Ag)	108.1681	49.5830 (CD/PEI/Ag)	2.181556
400	CD/PEI	−62.5118 (CD)	31.3796 (PEI)	−31.1322	22.7713 (CD/PEI)	−1.36717
	CD/PEI/Au	22.7713 (CDPEI)	23.1177 (Au)	45.889	30.4455 (CD/PEI/Au)	1.507251
	CD/PEI/Ag		69.946 (Ag)	92.7163	47.6370 (CD/PEI/Ag)	1.946309
200	CD/PEI	−48.2464 (CD)	15.5095 (PEI)	−32.7369	8.6168 (CD/PEI)	−3.79919
	CD/PEI/Au	8.6168 (CDPEI)	19.572 (Au)	28.1888	10.4703 (CD/PEI/Au)	2.692263
	CD/PEI/Ag		11.7338 (Ag)	20.3506	33.28038 (CD/PEI/Ag)	0.611489

doped carbon dots and carbon dots/plasmonic nano-hybrids have been investigated after incubations for 24 h, (see Fig. S7†). It's clear that a uniform staining and a bright fluorescence for the live cells were observed. Moreover, an increase in the brightness/intensity of fluorescence imaging has been observed upon the existence of plasmonic nanostructures than that of pure carbon dots, as depicted in Fig. S7.† An intense blue emission was detected after incubation with C-dots/PEI/Ag nanohybrids solution under the excitation of 366 nm, without showing any auto-fluorescence behaviour. The lowest emission intensity is detected after incubation with C-dots solution without showing any auto-fluorescence behaviour, as shown in Fig. S7.†

For the present study, the cyto-toxicity has been estimated using MTT assay, as illustrated in Fig. S8† indicated that no obvious variation of the cell viability is observed at exposure to a very lowest concentration of 200 μg ml^{-1} for each of C-dots; C-dots/PEI, C-dots/PEI/Au and C-dots/PEI/Ag nanohybrids. At a concentration of 200 μg ml^{-1} C-dots showed cell viability to *ca.* 95%. Moreover, the treatment with C-dots/PEI remains virtually unchanged in the cell viability as C-dots *ca.* 92%. Upon the conjugation with plasmonic nanoparticles such as, gold and silver nanoparticles, the cell viability was significantly dropped to *ca.* 89 and 70%, respectively.

3. Experimental

3.1. Materials

Citric acid monohydrate (CA, $C_6H_8O_7 \cdot H_2O$, 99.0%) and trisodium citrate dihydrate ($C_6H_5Na_3O_7 \cdot 2H_2O$) were purchased from LOBA Chemie. Ethelyenediamine (EDA, $NH_2CH_2CH_2NH_2$, 99.0%) was purchased from Alpha Chemika. Sodium borohydride ($NaBH_4$, 85%) was purchased from WinLab Ltd. Silver nitrate ($AgNO_3$, 99%), hydrogen tetrachloroaurate(III) ($HAuCl_4 \cdot 3H_2O$, 99.99%) and polyethyleneimine (PEI, 50 wt% solution in water, M_n 1200, M_w 1300) were purchased from Sigma Aldrich.

3.2. Methodology

3.2.1. Synthesis of highly fluorescent carbon dots. Nitrogen doped carbon dots (NC-dots) was prepared based on the microwave irradiation method that developed previously by He *et al.*[59] Briefly, mixture of citric acid (CA, 0.02 M) and ethylenediamine (EDA, 0.82 M) was dissolved ultrasonically into 100 ml of distilled water. A clear and light yellow solution was obtained. This mixture was transferred into a microwave oven (Olympic Electric, Model: KOG-1A4H) operated at 2450 MHz frequency, and power 1000 W. The reaction was carried out at power of 600 W for 13 minutes. Dark brown crude has been obtained at the bottom of the vessels. The product was purified for further characterization by dissolving into 100 ml distilled water, and then lyophilized using freeze dryer (Christ, ALPHA 2–4 LD plus, Germany) for 48 h to produce brownish powder.

3.2.2. Formation of plasmonic@spacer@C-dots hybrid nanocomposites. Plasmonic nanoparticles such as, gold (Au NPs) and silver (Ag NPs) nanoparticles were prepared *via* chemical reduction method, as described previously.[52,93–95] Carbon dots were coated with polyethylenimine (PEI) solution in water (50 wt%) under vigorous stirring for 180 min at 80 °C.[75]

Different stoichiometric ratios as a preliminary study from (1 : 1 to 1 : 20) of plasmonic nanostructures such as, gold and

silver nanoparticles have been used to fabricate the proposed nanocomposites from C-dots/plasmonic nano-hybrids. A selected ratio of (1 : 14) has been used in this study. Then the mixture was aged for 24 h with gentle shaking. The as prepared nano-hybrids were ready for characterization.

3.3. Characterization

Optical properties in terms of UV-Vis absorption and fluorescence spectra were obtained using a T80 (PG Instruments) double beam spectrophotometer and Shimadzu RF-5301PC Spectrofluorimeter, respectively. The absorption spectra were recorded in the range from 200 to 900 nm, with an increment of the wavelength about 0.2 nm. Also, the fluorescence spectra were recorded on range from 200 to 900 nm, with an increment of the wavelength about 0.2 nm, where samples were excited at wavelength of 366 nm using UV-lamp as excitation source. The quantum yields (QYs) of the prepared samples was determined by comparing the measured intensity compared to quinine sulphate in 0.1 M H_2SO_4 solution (QY = 54%) as a ref. 96–98. The quantum yield of samples were calculated according the following equation:

$$QY_{C\text{-}dots} = QY_{dye} \times \left(\frac{I_{C\text{-}dots}}{I_{dye}}\right) \times \left(\frac{\eta_{dye}{}^2}{\eta_{C\text{-}dots}{}^2}\right) \quad (2)$$

where, $QY_{C\text{-}dots}$ is the quantum yield of the C-dots and (QY_{dye}) is the quantum yield of dye. ($I_{C\text{-}dots}$) integrated emission band of the C. Dots and (I_{dye}) is the integrated emission band of dye, and ($\eta_{C\text{-}dots}$) is the refractive index of the C-dots and (η_{dye}) the refractive index of dye at the excitation wavelength.[97]

Transmission Electron Microscope (TEM) JOEL-JEM 2100 was used to investigate the micrograph of obtained samples under operating voltage 200 kV. The size distribution of sterilized C-dots, C-dots/PEI, C-dots/PEI/Au and C-dots/PEI/Ag were measured by Malvern zetasizer Nano ZS instrument with He/Ne laser (633 nm) at an angle of 173° collecting backscatter optics. In addition, X-ray diffraction (XRD) measurements have been carried out using a Philips X'Pert-Pro Powder Diffractometer operating with a Cu target with $K_{\alpha 1} = 1.54060$ Å, $K_{\alpha 2} = 1.5444$ Å.

3.4. Bio-compatibility test

3.4.1. Cell culture. Kidney epithelial cells (Vero cell line) derived from African green monkey as a model of normal cell line was obtained from ATCC (American tissue culture collection) and supplied by from the Holding Company for Biological Products & Vaccines (VACSERA), Cairo, Egypt. A monolayer of this cell line was maintained in Dulbecco's Modified Eagle's Medium (DMEM) supplemented with 10% fetal bovine serum (Biowest), antibiotics (2% penicillin–streptomycin (100 IU ml^{-1})), and 0.5% fungizone (Biowest). Then the cells subcultured by trypsinization (0.025% trypsin and 0.0025% EDTA; Biowest), and maintained in tissue culture laboratory at Virology & Immunology Unit, Cancer Biology Department, National Cancer Institute, Cairo, Egypt with cryogenic banking of low-passage cells to maintain uniformity of cell properties through the pervious study as reported by Schmidt and Emmons.[99] For each experiment, cells were sub-cultured, counted with hemo-cytometer and plated onto 96-well plates.[100]

3.4.2. Cell treatment and MTT assay. All materials were sterilized under UV irradiation for 3 h before their application in tissue culture. Serial dilutions were prepared in 2% DMEM giving concentrations at 200, 400, 600 and 800 μg ml^{-1} for plasmonic carbon dots hybrid nanocomposites (*i.e.* CD, CD/PEI, CD/PEI/Ag and CD/PEI/Au NPs) and at concentrations of 6.32, 12.5, 50 and 100 μg ml^{-1} for Au and Ag NPs, respectively. The cytotoxicity of all materials was tested against Vero cells by MTT assay (3-[4,5-dimethylthiazol-2-yl]-2,5-diphenyltetrazolium bromide dye (Serva electrophoresis, Germany)) that is based on the reduction of the dye by mitochondrial dehydrogenases of metabolically active cells to insoluble formazan crystals.[101–103] Exponentially growing cells were collected using 0.025% Trypsin–EDTA and plated in 96-well plates at 4000–5000 cells per well. Cells were exposed to all tested materials for 48 h. At the end of exposure, MTT solution in PBS (5 mg ml^{-1}) was then added to all wells including no cell blank and left to incubate for 90 min. Then DMSO (100 μl per well) was added to dissolve the formazan crystals with shaking for 10 min after which the absorbance was read at 590 nm against no cell blanks on a microplate reader (Biotek Model: ELX 800, USA).

Positive and negative controls were run in each plate. Negative controls (cells with media only; untreated cells) were set as 100% viable. Cells were subjected to osmotic shock (treated with distilled water) and served as positive controls (zero viability) and were used to subtract background from all OD values. The morphological changes of the cells were monitored by phase contrast microscopy (40× magnification).[100] The relative cell viability (%) related to control wells containing cells without nanomaterials was calculated by:

$$\text{Cell viability } (\%) = \frac{A_{test}}{A_{control}} \times 100 \quad (3)$$

where [A_{test}] is the absorbance of the test sample and [$A_{control}$] is the absorbance of control sample. Each result was the average of three wells, and 100% viability was determined from the untreated cells.

3.5. Live cell imaging

HepG-2 human liver cancerous cells obtained from the Holding Company for Biological Products & Vaccines (VACSERA), Cairo, Egypt, were cultured with high RMPI-1640 medium supplemented with 10% fetal bovine serum in a humidified incubator at 37 °C in which the CO_2 level was kept constant at 5%. For *in vitro* imaging based-on fluorescence microscopy, HepG-2 human liver cancerous cells were seeded in 6-well plate for 12 h before use. Then, the culture medium was replaced by 2.5 ml fresh medium containing 200 μg ml^{-1} of CDs, CD/PEI/Au and CD/PEI/Ag nano-hybrids. The cells were incubated for another 24 h then washed with isotonic PBS at pH 7.4 three times, and fixed with 4% paraformaldehyde solution in PBS at 4 °C overnight. The samples were examined using an epifluorescence microscope (Nikon) equipped with specific filters and a 100 W mercury lamp, and then directly observed with

fluorescence microscopy (Nikon, ECLIPSE Ti) under a 20× objective by UV light excitation at a wavelength ~366 nm.

4. Conclusions

Highly luminescent N-doped carbon dots was prepared *via* microwave irradiation method, and used to prepare C-dots/plasmonic nanohybrid such as, C-dots/PEI/Au and C-dots/PEI/Ag hybrid nanocomposites as an excellent candidates for biomedical imaging. The effect of plasmonic gold or silver nanoparticles on the optical properties of carbon dots in absence and in presence of six different polymeric dielectric spacers has been investigated. Our data show that the presence of PEI as surface passivation agent for the carbon dots enhances their emission properties due to the capping of surface defects and the traps. In addition, presence of plasmonic nanostructures such as, Au and Ag NPs displayed a significant enhancement in the optical absorptivity, quantum yield due to local field enhancement associated with the surface plasmon resonance in the metallic nanoparticles. The plasmonic-exciton coupling is more pronounced in the case of C-dots/Ag than that of the C-dots/Au nanocomposites due to the fact that there is a degree of overlap between the frequency of the surface plasmon resonance of silver nanoparticles and the carbon dots, while the SPR of gold nanoparticles is resonating far from the absorption of the carbon dots. Furthermore, biocompatibility assay and the response additivity showed that up to 800 μg ml^{-1} of C-dots/PEI/Au nano-hybrids could be used safely in diagnostic applications. This is indicated that the lowest dose of treatment using C-dots/PEI/Ag nano-hybrids (~200 μg ml^{-1}) could be used also in the diagnosis purposes. In addition, the cyto-toxicity based-on MTT assay showed that there is no significant sign of toxicity observed at exposure to a very low concentration 200 μg ml^{-1} using of C-dots, C-dots/PEI, C-dots/PEI/Au and C-dots/PEI/Ag nanohybrids. Our approach allows designing of multi-modal nano-hybrids combine properties for each of plasmonic nanostructures such as, Au and Ag NPs with C-dots to be used in a wide range of applications such as, chemical/biological sensing, probing and theranostics (*i.e.* therapy and imaging).

Acknowledgements

The Authors are gratefully appreciate Science and Technology Development Fund (STDF) for providing of the financial support through Grant ID: 6066, entitled "Novel Hybrid Carbon based Nanocomposites for Biosensors and Biomedical Imaging Applications", and grant ID: 1719, "Plasmonic-Semiconductor hybrid Nano-structural Solar Cells: toward Low Cost Great Enhancement of Solar Cell Efficiency".

Notes and references

1 G. Chen, *et al.*, (α-NaYbF4: Tm3+)/CaF2 core/shell nanoparticles with efficient near-infrared to near-infrared upconversion for high-contrast deep tissue bioimaging, *ACS Nano*, 2012, **6**(9), 8280–8287.
2 M. Chen, *et al.*, Inorganic fluorescent nanoprobes for cellular and subcellular imaging, *TrAC, Trends Anal. Chem.*, 2014, **58**, 120–129.
3 A. Burns, H. Ow and U. Wiesner, Fluorescent core–shell silica nanoparticles: towards "Lab on a Particle" architectures for nanobiotechnology, *Chem. Soc. Rev.*, 2006, **35**(11), 1028–1042.
4 U. Resch-Genger, *et al.*, Quantum dots versus organic dyes as fluorescent labels, *Nat. Methods*, 2008, **5**(9), 763–775.
5 J. Lippincott-Schwartz and G. H. Patterson, Development and use of fluorescent protein markers in living cells, *Science*, 2003, **300**(5616), 87–91.
6 M. Murakami, *et al.*, Fluorescence expression by bovine embryos after pronuclear microinjection with the EGFP gene, *J. Vet. Med. Sci.*, 1999, **61**(7), 843–847.
7 E. S. Swenson, *et al.*, Limitations of green fluorescent protein as a cell lineage marker, *Stem Cells*, 2007, **25**(10), 2593–2600.
8 P. Alivisatos, The use of nanocrystals in biological detection, *Nat. Biotechnol.*, 2004, **22**(1), 47–52.
9 C.-W. Kuo, *et al.*, Targeted nuclear delivery using peptide-coated quantum dots, *Bioconjugate Chem.*, 2011, **22**(6), 1073–1080.
10 A. Shiohara, *et al.*, Chemical reactions on surface molecules attached to silicon quantum dots, *J. Am. Chem. Soc.*, 2009, **132**(1), 248–253.
11 M. Dahan, *et al.*, Time-gated biological imaging by use of colloidal quantum dots, *Opt. Lett.*, 2001, **26**(11), 825–827.
12 J. P. Ryman-Rasmussen, J. E. Riviere and N. A. Monteiro-Riviere, Surface coatings determine cytotoxicity and irritation potential of quantum dot nanoparticles in epidermal keratinocytes, *J. Invest. Dermatol.*, 2007, **127**(1), 143–153.
13 Z. Yang, *et al.*, Controllable synthesis of fluorescent carbon dots and their detection application as nanoprobes, *Nano-Micro Lett.*, 2013, **5**(4), 247–259.
14 W. Khalil, *et al.*, Genotoxicity evaluation of nanomaterials: DNA damage, micronuclei, and 8-hydroxy-2-deoxyguanosine induced by magnetic doped CdSe quantum dots in male mice, *Chem. Res. Toxicol.*, 2011, **24**(5), 640–650.
15 M. Dahan, *et al.*, Diffusion dynamics of glycine receptors revealed by single-quantum dot tracking, *Science*, 2003, **302**(5644), 442–445.
16 M. Pelton, *et al.*, Evidence for a diffusion-controlled mechanism for fluorescence blinking of colloidal quantum dots, *Proc. Natl. Acad. Sci. U. S. A.*, 2007, **104**(36), 14249–14254.
17 Y.-F. Kang, *et al.*, Carbon quantum dots for zebrafish fluorescence imaging, *Sci. Rep.*, 2015, **5**, 11835.
18 X. T. Zheng, *et al.*, Glowing graphene quantum dots and carbon dots: properties, syntheses, and biological applications, *Small*, 2015, **11**(14), 1620–1636.
19 Y.-Q. Zhang, *et al.*, One-pot synthesis of N-doped carbon dots with tunable luminescence properties, *J. Mater. Chem.*, 2012, **22**(33), 16714–16718.
20 S. Y. Lim, W. Shen and Z. Gao, Carbon quantum dots and their applications, *Chem. Soc. Rev.*, 2015, **44**(1), 362–381.
21 S.-T. Yang, *et al.*, Carbon dots as nontoxic and high-performance fluorescence imaging agents, *J. Phys. Chem. C*, 2009, **113**(42), 18110–18114.

22 S. N. Baker and G. A. Baker, Luminescent carbon nanodots: emergent nanolights, *Angew. Chem., Int. Ed.*, 2010, **49**(38), 6726–6744.
23 S. Sahu, *et al.*, Simple one-step synthesis of highly luminescent carbon dots from orange juice: application as excellent bio-imaging agents, *Chem. Commun.*, 2012, **48**(70), 8835–8837.
24 B. De and N. Karak, A green and facile approach for the synthesis of water soluble fluorescent carbon dots from banana juice, *RSC Adv.*, 2013, **3**(22), 8286–8290.
25 Q. Liang, *et al.*, Easy synthesis of highly fluorescent carbon quantum dots from gelatin and their luminescent properties and applications, *Carbon*, 2013, **60**, 421–428.
26 S. C. Ray, *et al.*, Fluorescent carbon nanoparticles: synthesis, characterization, and bioimaging application, *J. Phys. Chem. C*, 2009, **113**(43), 18546–18551.
27 C. Liu, *et al.*, Nano-carrier for gene delivery and bioimaging based on carbon dots with PEI-passivation enhanced fluorescence, *Biomaterials*, 2012, **33**(13), 3604–3613.
28 L. Hu, *et al.*, Multifunctional carbon dots with high quantum yield for imaging and gene delivery, *Carbon*, 2014, **67**, 508–513.
29 J. Kim, *et al.*, Transfection and intracellular trafficking properties of carbon dot-gold nanoparticle molecular assembly conjugated with PEI-pDNA, *Biomaterials*, 2013, **34**(29), 7168–7180.
30 X. Li, *et al.*, Engineering surface states of carbon dots to achieve controllable luminescence for solid-luminescent composites and sensitive Be2+ detection, *Sci. Rep.*, 2014, **4**, 4976.
31 X. Michalet, *et al.*, Quantum dots for live cells, in vivo imaging, and diagnostics, *science*, 2005, **307**(5709), 538–544.
32 C. Ding, A. Zhu and Y. Tian, Functional surface engineering of C-dots for fluorescent biosensing and in vivo bioimaging, *Acc. Chem. Res.*, 2013, **47**(1), 20–30.
33 A. Sachdev, I. Matai and P. Gopinath, Implications of surface passivation on physicochemical and bioimaging properties of carbon dots, *RSC Adv.*, 2014, **4**(40), 20915–20921.
34 S. K. Das, *et al.*, Single-particle fluorescence intensity fluctuations of carbon nanodots, *Nano Lett.*, 2014, **14**(2), 620–625.
35 M. Baker, Nanotechnology imaging probes: smaller and more stable, *Nat. Methods*, 2010, **7**(12), 957.
36 S.-T. Yang, *et al.*, Carbon dots for optical imaging in vivo, *J. Am. Chem. Soc.*, 2009, **131**(32), 11308–11309.
37 Z. Liu and X.-J. Liang, Nano-carbons as theranostics, *Theranostics*, 2012, **2**(3), 235–237.
38 B. Kong, *et al.*, Carbon dot-based inorganic–organic nanosystem for two-photon imaging and biosensing of pH variation in living cells and tissues, *Adv. Mater.*, 2012, **24**(43), 5844–5848.
39 S. Qu, *et al.*, Ratiometric fluorescent nanosensor based on water soluble carbon nanodots with multiple sensing capacities, *Nanoscale*, 2013, **5**(12), 5514–5518.
40 S. Zhu, *et al.*, Highly photoluminescent carbon dots for multicolor patterning, sensors, and bioimaging, *Angew. Chem., Int. Ed.*, 2013, **52**(14), 3953–3957.
41 N. A. Kotov, *et al.*, Optical and Dynamic Properties of Gold Metal Nanomaterials, in *Nanoparticle Assemblies and Superstructures*, 2005, CRC Press. pp. 193–206.
42 S. Link and M. A. El-Sayed, Shape and size dependence of radiative, non-radiative and photothermal properties of gold nanocrystals, *Int. Rev. Phys. Chem.*, 2000, **19**(3), 409–453.
43 K.-S. Lee and M. A. El-Sayed, Gold and silver nanoparticles in sensing and imaging: sensitivity of plasmon response to size, shape, and metal composition, *J. Phys. Chem. B*, 2006, **110**(39), 19220–19225.
44 J. A. Creighton and D. G. Eadon, Ultraviolet-visible absorption spectra of the colloidal metallic elements, *J. Chem. Soc., Faraday Trans.*, 1991, **87**(24), 3881–3891.
45 W. A. Murray and W. L. Barnes, Plasmonic materials, *Adv. Mater.*, 2007, **19**(22), 3771–3782.
46 U. Kreibig and M. Vollmer, *Optical properties of metal clusters*, Springer Science & Business Media, 2013, vol. 25.
47 C. Burda, *et al.*, Chemistry and properties of nanocrystals of different shapes, *Chem. Rev.*, 2005, **105**(4), 1025–1102.
48 H. A. Atwater and A. Polman, Plasmonics for improved photovoltaic devices, *Nat. Mater.*, 2010, **9**(3), 205–213.
49 N. J. Halas, Plasmonics: an emerging field fostered by Nano Letters, *Nano Lett.*, 2010, **10**(10), 3816–3822.
50 A. Vora, *et al.*, Exchanging ohmic losses in metamaterial absorbers with useful optical absorption for photovoltaics, *Sci. Rep.*, 2014, **4**, 4901.
51 Y. Choi, *et al.*, Interface-controlled synthesis of heterodimeric silver–carbon nanoparticles derived from polysaccharides, *ACS Nano*, 2014, **8**(11), 11377–11385.
52 M. Amjadi, Z. Abolghasemi-Fakhri and T. Hallaj, Carbon dots-silver nanoparticles fluorescence resonance energy transfer system as a novel turn-on fluorescent probe for selective determination of cysteine, *J. Photochem. Photobiol., A*, 2015, **309**, 8–14.
53 R. D. Schmitz, J. O. Karolin and C. D. Geddes, Plasmonic enhancement of intrinsic carbon nanodot emission, *Chem. Phys. Lett.*, 2015, **622**, 124–127.
54 C. Li, *et al.*, Metal-enhanced fluorescence of carbon dots adsorbed Ag@ SiO 2 core-shell nanoparticles, *RSC Adv.*, 2012, **2**(5), 1765–1768.
55 C. Ran, *et al.*, A general route to enhance the fluorescence of graphene quantum dots by Ag nanoparticles, *RSC Adv.*, 2014, **4**(42), 21772–21776.
56 Y. Liu, *et al.*, Plasmon-enhanced photoluminescence of carbon dots–silica hybrid mesoporous spheres, *J. Mater. Chem. C*, 2015, **3**(12), 2881–2885.
57 Y. Dong, *et al.*, Polyamine-functionalized carbon quantum dots as fluorescent probes for selective and sensitive detection of copper ions, *Anal. Chem.*, 2012, **84**(14), 6220–6224.
58 Y. Liu, Y. Zhao and Y. Zhang, One-step green synthesized fluorescent carbon nanodots from bamboo leaves for copper (II) ion detection, *Sens. Actuators, B*, 2014, **196**, 647–652.
59 H. He, *et al.*, Rapid microwave-assisted synthesis of ultra-bright fluorescent carbon dots for live cell staining, cell-

specific targeting and in vivo imaging, *J. Mater. Chem. B*, 2015, **3**(24), 4786–4789.
60 M. Zheng, *et al.*, On–off–on fluorescent carbon dot nanosensor for recognition of chromium (VI) and ascorbic acid based on the inner filter effect, *ACS Appl. Mater. Interfaces*, 2013, **5**(24), 13242–13247.
61 Y. Zhang, *et al.*, Fluorescent probes for "off–on" highly sensitive detection of Hg 2+ and L-cysteine based on nitrogen-doped carbon dots, *Talanta*, 2016, **152**, 288–300.
62 G. Eda, *et al.*, Blue photoluminescence from chemically derived graphene oxide, *Adv. Mater.*, 2010, **22**(4), 505–509.
63 J. Ju, *et al.*, Nitrogen-doped graphene quantum dots-based fluorescent probe for the sensitive turn-on detection of glutathione and its cellular imaging, *RSC Adv.*, 2014, **4**(94), 52583–52589.
64 L. Li, *et al.*, Focusing on luminescent graphene quantum dots: current status and future perspectives, *Nanoscale*, 2013, **5**(10), 4015–4039.
65 Y. Dong, *et al.*, Carbon-Based Dots Co-doped with Nitrogen and Sulfur for High Quantum Yield and Excitation-Independent Emission, *Angew. Chem., Int. Ed.*, 2013, **52**(30), 7800–7804.
66 P. Yu, *et al.*, Temperature-dependent fluorescence in carbon dots, *J. Phys. Chem. C*, 2012, **116**(48), 25552–25557.
67 D. Pan, *et al.*, Observation of pH-, solvent-, spin-, and excitation-dependent blue photoluminescence from carbon nanoparticles, *Chem. Commun.*, 2010, **46**(21), 3681–3683.
68 S. Qu, *et al.*, A Biocompatible Fluorescent Ink Based on Water-Soluble Luminescent Carbon Nanodots, *Angew. Chem., Int. Ed.*, 2012, **51**(49), 12215–12218.
69 G. Xiaohui, *et al.*, One-pot synthesis of carbon nanodots for fluorescence turn-on detection of Ag+ based on the Ag+– induced enhancement of fluorescence, *J. Mater. Chem. C*, 2015, **3**, 2302–2309.
70 M. L. Mueller, *et al.*, Triplet states and electronic relaxation in photoexcited graphene quantum dots, *Nano Lett.*, 2010, **10**(7), 2679–2682.
71 J. Wang, C. F. Wang and S. Chen, Amphiphilic Egg-Derived Carbon Dots: Rapid Plasma Fabrication, Pyrolysis Process, and Multicolor Printing Patterns, *Angew. Chem.*, 2012, **124**(37), 9431–9435.
72 Y. Dong, *et al.*, Extraction of electrochemiluminescent oxidized carbon quantum dots from activated carbon, *Chem. Mater.*, 2010, **22**(21), 5895–5899.
73 J. Peng, *et al.*, Graphene quantum dots derived from carbon fibers, *Nano Lett.*, 2012, **12**(2), 844–849.
74 H. Dong, *et al.*, Polyol-mediated C-dot formation showing efficient Tb 3+/Eu 3+ emission, *Chem. Commun.*, 2014, **50**(56), 7503–7506.
75 B. Han, *et al.*, Polyethyleneimine modified fluorescent carbon dots and their application in cell labeling, *Colloids Surf., B*, 2012, **100**, 209–214.
76 Y.-P. Hsieh, *et al.*, Mechanism of giant enhancement of light emission from Au/CdSe nanocomposites, *Nanotechnology*, 2007, **18**(41), 415707.
77 T. Pons, *et al.*, On the quenching of semiconductor quantum dot photoluminescence by proximal gold nanoparticles, *Nano Lett.*, 2007, **7**(10), 3157–3164.
78 K. M. AbouZeid, M. B. Mohamed and M. S. El-Shall, Hybrid Au–CdSe and Ag–CdSe Nanoflowers and Core–Shell Nanocrystals via One-Pot Heterogeneous Nucleation and Growth, *Small*, 2011, **7**(23), 3299–3307.
79 M. Achermann, Exciton– plasmon interactions in metal–semiconductor nanostructures, *J. Phys. Chem. Lett.*, 2010, **1**(19), 2837–2843.
80 W. Deng, *et al.*, Metal-enhanced fluorescence in the life sciences: here, now and beyond, *Phys. Chem. Chem. Phys.*, 2013, **15**(38), 15695–15708.
81 P. B. Johnson and R.-W. Christy, Optical constants of the noble metals, *Phys. Rev. B: Solid State*, 1972, **6**(12), 4370.
82 J.-W. Liaw, H.-C. Chen and M.-K. Kuo, Comparison of Au and Ag nanoshells' metal-enhanced fluorescence, *J. Quant. Spectrosc. Radiat. Transfer*, 2014, **146**, 321–330.
83 J. Zhang, *et al.*, Metal-enhanced single-molecule fluorescence on silver particle monomer and dimer: coupling effect between metal particles, *Nano Lett.*, 2007, **7**(7), 2101–2107.
84 E. Dulkeith, *et al.*, Fluorescence quenching of dye molecules near gold nanoparticles: radiative and nonradiative effects, *Phys. Rev. Lett.*, 2002, **89**(20), 203002.
85 X. Kong, *et al.*, Synthesis and application of surface enhanced Raman scattering (SERS) tags of Ag@ SiO 2 core/shell nanoparticles in protein detection, *J. Mater. Chem.*, 2012, **22**(16), 7767–7774.
86 C. Li, *et al.*, Enhanced fluorescence of graphene oxide by well-controlled Au@ SiO2 core-shell nanoparticles, *J. Fluoresc.*, 2014, **24**(1), 137–141.
87 P. Anger, P. Bharadwaj and L. Novotny, Enhancement and quenching of single-molecule fluorescence, *Phys. Rev. Lett.*, 2006, **96**(11), 113002.
88 H. Cheng, *et al.*, Gold nanoparticle-enhanced near infrared fluorescent nanocomposites for targeted bio-imaging, *RSC Adv.*, 2015, **5**(1), 20–26.
89 S. A. Loutfy, *et al.*, Anti-proliferative Activities of Metallic Nanoparticles in an in Vitro Breast Cancer Model, *Asian Pacific Journal of Cancer Prevention*, 2015, **16**(14), 6039–6046.
90 P. AshaRani, *et al.*, Cytotoxicity and genotoxicity of silver nanoparticles in human cells, *ACS Nano*, 2008, **3**(2), 279–290.
91 J. Foucquier and M. Guedj, Analysis of drug combinations: current methodological landscape, *Pharmacol. Res. Perspect.*, 2015, **3**(3), e00149.
92 J. Bernhardt, *et al.*, Prespecified Dose-Response Analysis for A Very Early Rehabilitation Trial (AVERT), *Neurology*, 2016, **86**(23), 2138–2145.
93 J. Turkevich, G. Garton and P. Stevenson, The color of colloidal gold, *Journal of colloid Science*, 1954, **9**, 26–35.
94 J. Turkevich, P. C. Stevenson and J. Hillier, A study of the nucleation and growth processes in the synthesis of colloidal gold, *Discuss. Faraday Soc.*, 1951, **11**, 55–75.
95 H. Shaat, *et al.*, Modified gold nanoparticles for intracellular delivery of anti-liver cancer siRNA,

International journal of pharmaceutics, 2016, **504**(1), 125–133.

96 S. Chandra, *et al.*, Luminescent S-doped carbon dots: an emergent architecture for multimodal applications, *J. Mater. Chem. B*, 2013, **1**(18), 2375–2382.

97 J. R. Lakowicz, *Principles of fluorescence spectroscopy*, Springer Science & Business Media, 2013.

98 S. Mitra, *et al.*, Room temperature and solvothermal green synthesis of self passivated carbon quantum dots, *RSC Adv.*, 2013, **3**(10), 3189–3193.

99 N. J. Schmidt and R. W. Emmons, *Diagnostic procedures for viral, rickettsial and chlamydial infections*, American Public Health Association, 1989.

100 S. A. Loutfy, *et al.*, Synthesis, characterization and cytotoxic evaluation of chitosan nanoparticles: in vitro liver cancer model, *Adv. Nat. Sci.: Nanosci. Nanotechnol.*, 2016, **7**(3), 035008.

101 F. Du, *et al.*, A low cytotoxic and ratiometric fluorescent nanosensor based on carbon-dots for intracellular pH sensing and mapping, *Nanotechnology*, 2013, **24**(36), 365101.

102 N. Puvvada, *et al.*, Synthesis of biocompatible multicolor luminescent carbon dots for bioimaging applications, *Sci. Technol. Adv. Mater.*, 2016, 045008.

103 ISO, I. 10993-05, *Biological evaluation of medical devices—Part 5: tests for in vitro cytotoxicity*, ISO 10993-12: 2007, International Organization for Standardization, 2009.